METALLURGICAL & MATERIALS TRANSACTIONS A 36A (2005) 3281–3289

In-situ Observations of Lattice Parameter Fluctuations in Austenite and Transformation to Bainite

S. S. Babu

Formerly at Metals and Ceramics Division, Oak Ridge National Laboratory

Oak Ridge, TN 37831 USA, Currently at Edison Welding Institute, Columbus, Ohio 43017, USA

E. D. Specht and S. A. David

Metals and Ceramics Division, Oak Ridge National Laboratory

Oak Ridge, TN 37831 USA

E. Karapetrova and P. Zschack

Frederick Seitz Materials Research Laboratory

University of Illinois at Urbana-Champaign

Urbana, Illinois 61801, USA

M. Peet and H. K. D. H. Bhadeshia

Department of Materials Science and Metallurgy

University of Cambridge, CB23QZ

UK

Corresponding Author: S. S. Babu, suresh_babu@ewi.org; Tel: (614) 688-5206

Final version after the acceptance: Revised version after the comments from the reviewers of Metallurgical and Materials Transactions 2005

Abstract

The isothermal transformation of high carbon austenite to bainitic ferrite has been investigated with the *in situ* technique of time-resolved X-ray diffraction using synchrotron radiation. The measurements indicate that prior to transformation, the austenite divided into regions with significantly different lattice parameters. It is possible that this is due to the development of carbon-rich and carbon-poor regions in the austenite, as a precursor to transformations including the bainite reaction. The lattice parameter became uniform as transformation progressed and the fraction of carbon-poor austenite decreased. The ferrite itself exhibited a large range of lattice parameters during the early stages of transformation, due to the trapping of carbon.

Keywords

Steels, Phase Transformations, Bainitic transformations, Time-resolved X-ray diffraction and Transformation Kinetics

Introduction

The role of carbon during the transformation of austenite to bainitic ferrite in steels is interesting from a fundamental as well as a technological viewpoint. It is possible that bainite forms without diffusion and carbon subsequently redistributes or precipitates as carbides [1,2]. An alternative interpretation is that the ferrite grows with its equilibrium carbon concentration [3,4]. Historically, it has also been speculated that the austenite becomes heterogeneous with carbon-enriched and carbon-depleted regions, so that ferrite formation initiates in the carbon-depleted regions [5–11]. In the present work, it has been possible to follow the lattice parameter changes associated with the austenite at any temperature and during the course of the bainite transformation. If the changes can be attributed to solute concentration then they help interpret the role of carbon.

Experimental

The chemical composition of the steels used in this investigation is Fe - 0.75C – 1.63Si – 1.95Mn – 0.29Mo – 1.48Cr – 0.1V – 0.01Al – 0.003P – 0.003S wt%. This steel was selected because, the transformation rate is slow due to high carbon concentration and there are no other transformations including carbide precipitation that interfere with the formation of the bainitic ferrite [12]. The microstructure following isothermal transformation is a mixture of bainitic ferrite and carbon-enriched retained austenite. The silicon concentration is sufficiently high to prevent the precipitation of cementite from the austenite, as would normally occur in the upper bainite transformation temperature range [1].

Rectangular samples [2 × 4 × 95 mm] were made from this high-strength steel bar, which was homogenized at 1200°C for 48 hrs, for the diffraction experiments. It is important to note that after this homogenization treatment, the microstructure of the samples were essentially martensitic and with small amounts of retained austenite. Room temperature X-ray diffraction measurements also failed to show any texture in these samples. These homogenized samples were then heat-treated in-situ in a synchrotron beam line using resistive heating method.

The samples were heated to 1273 K and held at that temperature for 4 minutes. Then the steel was cooled at a rate of 10 K s^{-1} from 1273 K to 573 K and held at that temperature for 12 hrs. The temperature was controlled using direct resistive-heating using a type S (Pt/Pt10%Rh)

thermocouple. Oxidation was reduced by covering the sample with an inverted can filled with He.

Bending magnet synchrotron radiation was provided by beam line X33-BM-B at the Advanced Photon Source (Argonne, Illinois). A double-crystal Si(111) monochromator selected and sagitally focused to 30 keV X rays. At this energy, the penetration depth in steel is 0.16 mm. Slits defined a beam 0.25 mm high and 1.0 mm wide on the sample. The incident beam was carefully positioned well within the uniform temperature region of the sample. X rays were incident on the sample surface at a glancing angle of 5°. A schematic illustration of the experiment and a typical diffraction image is shown in Fig. 1. Diffracted X- rays were measured using a 1024x1024 pixel, Peltier-cooled, 16 bit CCD detector with a 60x60 μm^2 pixel size covering Bragg angles between 10° and 21°. 2x2 binning was used to speed detector readout. Assuming ideal diffraction geometry, the instrument resolution is estimated to be 0.005 to 0.015 Å for a given interplanar spacing of 0.5 to 2.5 Å, respectively. The minimum time resolution that can be attained in this set up without deterioration of signal to noise ratio was found to be 3 s. Therefore, in early stages of transformation the time resolution was set to 3 s and at the later stages of transformation the time resolution was increased to 34 s. The powder diffraction rings were integrated to give 1D scans of intensity versus interplanar spacing [13, 14].

The samples after the transformation were characterized by optical microscopy, automated hardness testing equipment and Philips XL-30FEG scanning electron microscopy. The energy dispersive X-ray mapping was performed with 250 nm intervals with 20 s dwell time while operating at 15 kV on a polished surface.

In addition to results from these heat-treatment experiments, the current work also utilized some of the published in-situ diffraction results measured during welding from another steel [15]. These measurements were performed at Stanford Synchrotron Radiation Laboratory and the time-resolution for this experiment was 0.05s.

Results and Discussions

Analyses of Transformation Kinetics

The dynamics of phase transformations from austenite to bainitic ferrite were monitored with the *in situ* time-resolved X-ray diffraction technique using synchrotron radiation in two samples. The crystal structure of austenite is face-centered cubic (FCC) and that of ferrite is body-centered cubic (BCC). A series of thousands of diffraction rings from $\{111\}_{FCC}$, $\{011\}_{BCC}$ and $\{002\}_{FCC}$ at different time intervals were integrated into an image format as a function of time at the isothermal transformation temperature. The diffraction results from two samples are summarized in Fig. 2. The images show changes in the diffraction patterns and lattice parameter changes during the isothermal hold at 573 K from 10 to 30000 s. For sample 1, the image [see Fig 2*a*] shows only the $\{111\}_{FCC}$ and $\{002\}_{FCC}$ diffraction peaks in the early stages of isothermal heat treatment. This diffraction evidence shows that the sample is fully austenitic on reaching 573 K. With increasing time at 573 K, the width of the $\{111\}_{FCC}$ peak increases and the intensity distribution becomes bimodal at the point indicated by an arrow "A" in the plot. This occurs before any detectable transformation to ferrite. Ferrite eventually appears, as indicated by [see Arrow B] the faint diffracted intensity from $\{011\}_{BCC}$. At this stage, the width of $\{002\}_{FCC}$ diffraction peaks also increased. In sample 2, the image [see Fig. 2*b*] shows predominantly $\{111\}_{FCC}$ and $\{002\}_{FCC}$ diffraction peaks and a weak $\{011\}_{BCC}$ diffraction peak

at the early stages of transformation. The widths of both $\{111\}_{\mathbf{FCC}}$ and $\{002\}_{\mathbf{FCC}}$ diffraction peaks are large and each has a bimodal intensity distribution (peak "splitting"). Analysis showed that the splitting of $\{111\}_{\mathbf{FCC}}$ peaks occurred during cooling from high temperatures to the isothermal transformation temperature. At longer times at 573 K, the ferrite fraction increased and the positions of the FCC diffraction peaks moved towards higher interplanar spacings. The lattice parameter of the austenite became more uniform as the ferrite fraction increased, as shown by arrows "A" and "B" in the images.

Comparison of results in figure 2 shows subtle differences in the measurements from the samples 1 and 2 before reaching the isothermal temperature, even though the samples are of the same composition and were subjected to similar heat-treatment. It is speculated that this difference could be due to local differences in austenite grain structure during cooling. Further high-speed X-ray diffraction characterization during continuous cooling is needed to evaluate the possible causes for these differences.

The data shown in the Fig. 2 measured during isothermal treatment were further analyzed by fitting a Gaussian peak to all the individual ferrite and austenite diffraction peaks of the form.

$$I = I_o \exp\left\{\left(\frac{d - d_o}{w}\right)^2\right\} \qquad (1).$$

I corresponds to the observed diffraction intensity as a function of interplanar spacing, I_0 is the intensity for a given mean interplanar spacing d_0 and w is given by the Gaussian peak width. In addition, the areas under the $\{111\}_{\mathbf{FCC}}$ and $\{011\}_{\mathbf{BCC}}$ peaks were also calculated. The integrated areas were converted to phase fraction by considering structure factor, multiplicity factor, Lorentz polarization and temperature factor with the standard methodology [16].

The variations of mean interplanar spacing for **FCC** {111} (d_{111}) and **BCC** {011} (d_{011}) planes and width of **FCC** {111} (w_{111}) and **BCC** {011} (w_{011}) peaks are shown in Fig. 3. In both samples, d_{111} increased with increase in ferrite fraction, as expected from the partitioning of carbon into the austenite. In sample 1, before the onset of the austenite to bainitic ferrite transformation, d_{111} slightly increased from 2.095 Å to 2.098 Å within the time period 10 to 300-s, this being accompanied by an increase in w_{111} from 0.008 to 0.009 Å. Although this increase was within the estimated instrument resolution of 0.015 Å, the observed increase w_{111} was very systematic. This systematic increase is puzzling given that the change occurs in the absence of transformation. With sample 2, d_{111} increased slightly from 2.099 Å to 2.101 Å within the time period of 10 to 100-s, as the ferrite fraction increased slightly from 0.05 to 0.07. During this period, w_{111} remained constant at a higher value of 0.014 Å; this larger value compared with sample 1 is simply due to some ferrite forming in the sample before the transformation temperature was reached. In conjunction with these measurements, at the early stages of isothermal holding until 100s, temperature fluctuations were also observed in both experiments. However, these fluctuations (see Figure 6) reduced after 100s, however, the austenite diffraction peaks showed some anomalous behavior. These unusual variations of widths of austenite diffraction peaks will be analyzed in depth later in this paper.

In sample 1, d_{011} systematically decreased from 2.047 Å to 2.044 Å as the isothermal holding time increased from 614 to 30000 s. This is indeed expected, since the ferrite initially is supersaturated with carbon, some of which then partitions into the austenite, leading to a decrease in the ferrite lattice parameter. At any given time, the ferrite lattice parameter may have

a wide range of values as the ferrite carbon concentration within plates that have formed at different times. As a result, w_{011} increases from 0.009 Å to 0.015 Å; this interpretation might seem inconsistent with the observations on sample 2 (where d_{011} goes through a maximum), but it is important to note that in that case, w_{111} is much larger, possibly because due to a more nonuniform distribution of carbon in the parent austenite. For this reason, w_{011} from the sample 2 is also larger than sample 1, due to the corresponding greater range of carbon in the ferrite.

Assuming that the lattice parameter variations can be attributed to carbon concentration, the latter can be estimated for ferrite using d_{011}. Using a published relationship that relates the ferrite lattice parameter to alloying element concentrations [17,18], the carbon in ferrite was estimated for both sample 1 and sample 2. The calculation technique is described below.

$$d_{\{011\}}^{BCC} = a_{BCC} / \sqrt{2}$$

$$a_{BCC} = 2.8664 + \frac{\left(a_{Fe} - 0.279 M_C\right)^2 \left(a_{Fe} + 2.496 M_C\right) - a_{Fe}^3}{3 a_{Fe}^2} - 0.03 M_{Si} + 0.06 M_{Mn} + 0.07 M_{Ni} + 0.31 M_{Mo} + 0.05 M_{Cr} + 0.096 M_V \quad (2)$$

In the above equation, M_i corresponds to the mole fraction of elements *"i"* in the ferrite. Since the mobility of substitutional atoms is very sluggish at 573 K, the mole fractions of Si, Mn, Ni, Mo, Cr, and V are made equal to their nominal concentrations in the alloy. The lattice parameter of pure iron (a_{Fe}) is 2.8664 Å. In addition, to calculate the lattice parameter at 573 K, the thermal expansion coefficient of ferrite was derived from the diffraction data from on-heating measurements and was found to be 1.3864×10^{-5} K^{-1}. With the above equation, the range of carbon concentration was found to be 1.8 to 2.8 at. % (0.4 to 0.62 wt.%) for both samples during the isothermal transformation. This is consistent with recent observations using an atom probe [12], which revealed a range in ferrite of 0.15 to 2.27 at% (0.03 to 0.5 wt.%).

The optical microstructure and hardness variations from the same sample are shown in Fig. 4. The low magnification micrograph shows an island of untransformed region [see Fig. 4*a*]. Similar regions were found throughout the sample and are attributed to the untransformed austenite, which is stabilized by the partitioning of carbon from supersaturated ferrite [12]. The same micrograph shows that there is no significant carbon depletion due to decarburization from the surface. Moreover, the micrograph shows the presence of a thin layer of oxide on the surface of the sample. This indeed was detected by the diffraction measurements and identified as predominantly magnetite ($Fe_{2.9}O_4$) and small amounts of hematite (Fe_2O_3). Possible overlapping of austenite and oxide peaks during analysis were also ruled out based on the measured intensity from the oxide peaks. A high magnification micrograph [see Fig. 4*b*] showed the presence of both martensite and bainitic microstructure. Spatial hardness [see Fig. 4*c*] measurements showed large variations in the hardness with some regions of hard spots.

Analyses of Austenite Diffraction Peaks

The variation of w_{111} in sample 1 prior to transformation, and the large value of w_{111} in sample 2 are now discussed. It may not be justified to treat the {111} data as a single peak, as shown in Figure 5 but rather as the superposition of two peaks, both originating from the austenite. This is referred to here as "peak splitting" as might occur if carbon-rich and carbon-poor regions develop spontaneously. The deconvolution of the data in Figure 5 was done using a Gaussian

shape[†]. Similar splitting was also observed in the {002}-austenite peaks. The intensity of the low d_{111} peak decreases as ferrite develops, which would be consistent with the elimination of low-carbon austenite which transforms first, and due to any enrichment of the austenite with carbon partitioned from bainitic ferrite (Figure 5). The data can also be used to estimate phase fractions, as shown in Figure 6. The temperature fluctuations are seen to cause corresponding changes in the measured lattice spacings. As stated before, the fraction of the smaller lattice parameter austenite decreased as ferrite formed.

The carbon concentrations of the two types of austenite can be estimated if it is assumed that parameter variations are due to carbon variations. The calculation technique is described below. From the published relationship [17,18] between the austenite composition and lattice parameter at room temperature (300 K) ($a_{\mathbf{FCC}}$), the carbon concentrations of these austenite regions can be estimated.

$$d_{\{111\}}^{FCC} = a_{FCC} / \sqrt{3}$$
$$a_{FCC} = 3.5780 + 0.033x_c + 0.00095x_{Mn} - 0.0002x_{Ni} + 0.0006x_{Cr} + 0.0056x_{Al} + 0.0031x_{Mo} + 0.0018x_V \quad (3).$$

In the above equation x_i corresponds to the weight percent of elements *"i"* in the austenite. In addition, to calculate the lattice parameter at 573 K, an estimate of the thermal expansion coefficient of austenite is necessary. The thermal expansion coefficient of austenite was measured to be 2.5032×10^{-5} K^{-1} from the on-cooling diffraction data. It is important to note that the measured thermal expansion coefficient of austenite is higher than other low-carbon steels (1.9×10^{-5} K^{-1}) measured using dilatometer techniques [19]. Recently, Acet et al [20] reported thermal expansion coefficient of austenite higher than 2×10^{-5} K^{-1} in simple Fe-C steels. The high thermal expansion coefficient in the current steels is tentatively attributed to high cooling rate and also high carbon concentrations. Using the measured thermal expansion coefficient, the lattice parameter at 573 K was calculated for both low- and high-carbon austenite regions of the sample 1. After 300 s isothermal hold, the carbon-poor austenite region corresponds to 0.62 wt.% C and the carbon-rich austenite to 1.03 wt.% C. It is interesting that the ferrite carbon concentration ranges from 0.40 to 0.62 wt.%. This may be because it is the low-carbon austenite that transforms first, an interpretation, which would be consistent with the suggestions of Klier and Lyman [5], Entin [6] and recently by Wu et al. [11].

Other Mechanisms for Peak Splitting

Before the discussion of the mechanisms for this peak splitting, it is important to comment on the use of simple symmetric Gaussian peak fitting in the previous section. It is important to note that asymmetry of diffraction peaks may develop due to the presence of internal stresses and dislocation characteristics within the grain of any alloy [21]. Because the current isothermal heat-treatments were done without any mechanical deformation, the use of symmetric Gaussian peaks is assumed to be valid. In addition, the data from sample 1 also showed the enhancement of peak splitting (or asymmetry) during isothermal hold [see Fig. 6*a*], which can not be explained based on the generation of certain types of dislocations during isothermal hold. In this section, other possible causes of the peak splitting are discussed.

[†] The dynamics of peak splitting shown in Fig. 5 are shown in a movie format at the following location: http://mjndeweb.ms.ornl.gov/BES/Supplement/Peak/BabuetalPaper.htm

(1) The lattice parameter of austenite is also depends on substitutional solutes [Equation 3]. Any variation in substitutional solute content could in principle lead to corresponding changes in the austenite lattice parameter. Although the alloy used had been given a homogenization heat treatment to minimize the presence of any solidification-induced chemical segregation, there may remain residual variations, which were characterized energy dispersive X-ray peak intensity mapping. The peak intensities of Si, Mn, Cr and Fe are mapped from a local region of the samples heat-treated at 573 K [see Fig. 7]. In these grey scale images, the maximum intensity corresponds to white color and the zero intensity corresponds to black color. The maps shown only random variations and do not correlate with the observed microstructure. On comparing to the intensity of iron peaks, these random variations are not significant, and certainly not large enough (equation 3) to cause peak splitting. Atom probe compositional analysis in the same steel after similar heat-treatments in many different regions failed to show any change in the nominal concentration of substitutional element concentration [12].

Notice that any form of substitutional solute segregation present in the austenite cannot in any case explain why the austenite, during isothermal holding, first has a single lattice parameter, which splits into two peaks as a function of time.

(2) Carbon concentration gradients may develop if the carbides precipitate from the austenite during cooling from austenitizing temperature. However, the alloy is designed with a high silicon content, precisely to avoid carbides. Extensive electron microscopy and atom probe microscopy analysis of the same steel has demonstrated the absence of carbides in the microstructure [12].

(3) One possibility is decarburization from the surface of the sample contributing to carbon variations in the austenite. Careful optical microscopy and hardness measurements failed to show any decarburization. Again, this cannot explain why the austenite, during low-temperature isothermal holding following austenitisation, first has a single lattice parameter, which splits into two peaks as a function of time. In addition, the decarburization also will lead to peak broadening not *peak splitting*.

(4) Substitutional atom might diffuse via some sort of a spinodal within the 400 s of the observed lattice parameter fluctuations at 573 K. However, the diffusivities of substitutional elements ranges from 1 x 10^{-29} to 1 x 10^{-31} m^2s^{-1} in the austenite phase at 573 K compared to a carbon diffusivity of 8 x 10^{-19} m^2s^{-1} [22]. The estimated diffusion distance ($2\sqrt{D_i t}$) for substitutional atoms for 400 s at 573 K in austenite is 1 x 10^{-14} to 1 x 10^{-13} m, which is less than the interatomic distance. In contrast, the diffusion distance for carbon atoms is expected to be 36 nm. Therefore, the observed austenite diffraction peak splitting after reaching 573 K cannot be attributed to diffusion of substitutional atoms.

(5) A particle size L will give a diffraction peak width $w=0.6d^2/L$; w_{111}=0.01 Å corresponds to L=260 Å. While the ferrite would be expected to nucleate with a small particle size within the austenite, there is no reason to expect such a dramatic decrease in the austenite particle size in the early stages of transformation. An inhomogeneous stress distribution with Gaussian width w_{stress} will give peak width $w=w_{stress}d/G$, where G=75 GPa is the shear modulus of austenite. w_{111}=0.01 Å corresponds to w_{stress}=360 MPa. Transformation stresses might be this large in the small fraction of ferrite, but not in the bulk of the austenite. However, during the formation of plate shaped ferrite, the strains can be accommodated entirely in the austenite [23]. These strains will not be uniform, increasing with magnitude as the plate shape is reached. Moreover, these two sources of *broadening* would not be expected to produce a peak *splitting*.

(6) A possible cause of carbon partitioning in austenite is spinodal decomposition. A solid solution can become heterogeneous by spinodal decomposition, if the enthalpy of solution is such that it favors the clustering of like atoms; in these circumstances, the free energy of mixing can show two minima as a function of concentration, leading to the possibility of spinodal decomposition at low temperatures. The molar Gibbs energy of austenite and ferrite as a function of carbon concentration was calculated using ThermoCalc® software [24] and Thermo-Tech Iron database [25] [see Fig. 8]. The second derivative of Molar Gibbs energy (d^2G/dx^2) of austenite with respect to carbon concentration was always positive [26], a condition inconsistent with the existence of a spinodal. This is inconsistent with our tentative conclusion that the lattice parameter fluctuations are associated with carbon concentration variations on an unspecified scale, but one could argue that the thermodynamic data on which the calculations are based are not appropriate for such low temperatures.

(7) One further possibility is the classical two electronic states model for austenite, in which there is co-existence of high and low molar volume states of austenite at any temperature; the apparently large thermal expansivity of austenite is because the fraction of each state is temperature dependent [27]. Unfortunately, this does not involve a time-dependence, which is what has been detected in the present experiments, and indeed, the phenomenon is independent of the presence of carbon.

Measurements in Other Alloys

Suppose the interpretation of the synchrotron data is correct and that austenite does become non-uniform prior to transformation, it is relevant to ask whether this effect is general or specific to the alloy studied. In this context, previously published time-resolved in-situ diffraction data from the Fe- 0.23 C- 1.77Al- 0.56 Mn wt.% steel, obtained during weld cooling, [15] was reanalyzed. The analysis is presented in Figure 9. The left plot shows the intensity of austenite and ferrite diffraction peaks measured at a time-resolution of 0.05 s using synchrotron radiation. At high temperature, only the $\{111\}_{\mathbf{FCC}}$ austenite peak is present. As the weld cools down the austenite lattice shrinks and at a critical time, the austenite diffraction peak splits into two peaks. The austenite peak with high 2θ (low d-spacing) and low 2θ (high d-spacing) is interpreted as the formation of low-carbon and high-carbon austenite. With continued cooling, the diffraction peaks from low-carbon austenite decreases with a concurrent increase in ferrite $\{110\}_{\mathbf{BCC}}$ diffraction intensity. With continued cooling, the high-carbon austenite also transforms. The quantitative analysis of the diffraction data is shown in right side of the Fig. 9 and shows that the trends are consistent, that on cooling, the “low-carbon” austenite disappears first. It is possible therefore that the observations made here are general.

Conclusions

Transformation kinetics and lattice parameters were measured during isothermal transformation of a high-carbon austenite to bainitic ferrite using time-resolved X-ray diffraction technique using Synchrotron radiation. The analyses of diffraction peaks indicated splitting of austenite peaks before the onset of ferrite transformation. This peak splitting was tentatively attributed to the development of carbon-rich and carbon-poor regions in the austenite. The fraction of carbon-poor austenite region gradually decreased with the on-set of bainitic ferrite transformation. At the early stages of transformation, the diffraction data from ferrite also exhibited a large range of lattice parameters indicating possible carbon trapping. With continued isothermal holding, as the

transformation progressed, the austenite lattice parameters became more uniform and increased to higher value. Reanalysis of a published time-resolved X-ray diffraction data from a steel weld with different composition showed similar austenite splitting and the disappearance of low-carbon austenite with the on-set of bainitic ferrite transformation, suggesting that this phenomenon may be general.

Acknowledgements

Research sponsored by the Division of Materials Sciences and Engineering, U. S. Department of Energy, under Contract DE-AC05-00OR22725 with UT-Battelle, LLC. The UNICAT facility at the Advanced Photon Source (APS) is supported by the U.S. DOE under Award No. DEFG02-91ER45439, through the Frederick Seitz Materials Research Laboratory at the University of Illinois at Urbana-Champaign, the Oak Ridge National Laboratory (U.S. DOE contract DE-AC05-00OR22725 with UT-Battelle LLC), the National Institute of Standards and Technology (U.S. Department of Commerce) and UOP LLC. The APS is supported by the U.S. DOE, Basic Energy Sciences, Office of Science under contract No. W-31-109-ENG-38. The authors at University of Cambridge are grateful to the Engineering and Physical Sciences Research Council, CORUS and The Worshipful Company of Ironmongers for supporting this research. The authors also thank Dr. E. A. Kenik for help with scanning electron microscopy EDS mapping.

Reference

1. H. K. D. H. Bhadeshia: "Bainite in Steels," 2nd Edition, IOM Communications Ltd, London, 2001.
2. J. W. Christian: "The theory of transformations in metals and alloys,' 3rd Edition, Part 11, Pergamon Press, London, 2002.
3. M. Hillert *Scripta Materialia*: 2002, **47**, 175.
4. H. I. Aaronson, W. T. Reynolds, G. J. Shiflet and G. Spanos: *Metallurgical Transactions A* , 1990, **21**, 1343.
5. E. P. Klier and T. Lyman: *Transactions of the American Institute of Mining and Metallurgical Engineers*, 1944, **158**, 394-422.
6. Eintin RI. The elementary reactions in the austenite->pearlite and austenite->bainite transformations, in the proceedings of Decomposition of austenite by diffusional processes, Eds. V. F. Zackay and H. I. Aaronson, Interscience Publishers, New York, 1962.
7. Bojarski Z and Bold T. *Acta Metallurgica*, 1974, **22**, 1223 – 1234.
8. Lim C and Wutting M. *Acta Metallurgica*, 1974, **22**, 1215 – 1222.
9. Zhang JH, Chen SC and Hsu TY. *Acta Metallurgica*, 1989, **37**, 241.
10. Wu XL, Jia H, Zhang X and Kang M. *J. Mater. Sci. Technol.*, 1995, **11**, 353.

11. Wu XL, Zhang XY, Kang MK, Meng XK, Yang YQ and Han D. *Materials Transactions, JIM.,* 1994, **35**, 782.
12. Peet M, Babu SS, Miller MK and Bhadeshia HKDH, *Scripta Materialia*, 2004, **50**, 1277-1281.
13. Hammersley AP, Svensson SO, Hanfland M, Fitch AN and Häusermann D. *High Pressure Research*, 1996, **14**, 235.
14. Hammersley AP., *ESRF Internal Report*, **ESRF97HA02A**, Fit2D: An Introduction and Overview, 1997.
15. Babu SS, Elmer JW, Vitek JM, and David SA. *Acta Materialia*, 2002, **50**, 4763.
16. Cullity BD "Elements of X-ray diffraction," Addison-Wesley Publishing Inc., Massachusetts, 1978.
17. Bhadeshia HKDH, David SA, Vitek JM and Reed RW. *Materials Science and Technology*, 1991, **7**, 686.
18. Dyson DJ and Holmes B, *Journal of the Iron and Steel Institute*, 1970, **208**, 469.
19. S. S. Babu, "Acicular ferrite and bainite in Fe-Cr-C weld deposits," Ph.D. Thesis, University of Cambridge, 1992.
20. Acet M, Gehrmann B, Wassermann EF, Bach H, and Pepperhoff W, *J. of Magnetism and Magnetic Materials*, 2001, **232**, 221.
21. Barabash OM, Babu SS, David SA, Vitek JM and Barabash RI, *Journal of Applied Physics*, 2003, **94**, 738.
22. Borgenstam A, Engstrom T, Hoglund L, Shi PF, and Sundman B. *Calphad*, 2000, **21,** 269-280.
23. Christian JW, "The theory of transformations in metals and alloys – Part 1," Pergamon Press, Elsevier Science, New York, 2002, p. 461.
24. Andersson JO, Helander T, Hoglund L, and Sundman B. *CALPHAD*, 2002, **26**; 273.
25. Thermotech Fe-Data Thermodynamic Database, Thermotech Ltd / Sente Software Ltd., UK.
26. Cahn JW. *Acta Metallurgica*, 1961, **9**, 795.
27. Kaufman L, Clougherty EV, Weiss RJ, *Acta Metallurgica,* 1963, **11**, 323.

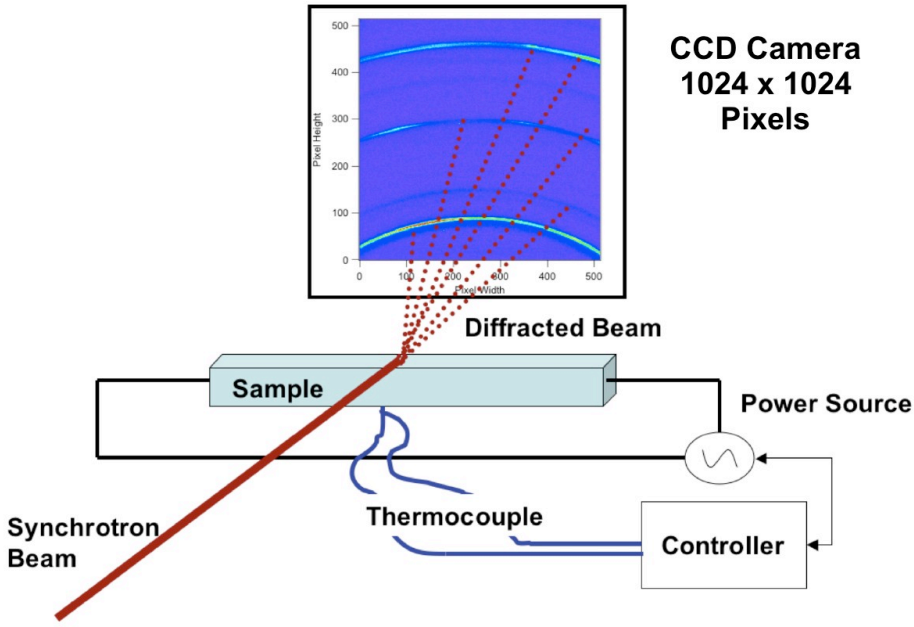

Figure 1. Schematic illustration of experimental setup and in-situ diffraction measurements in a synchrotron beam line is shown.

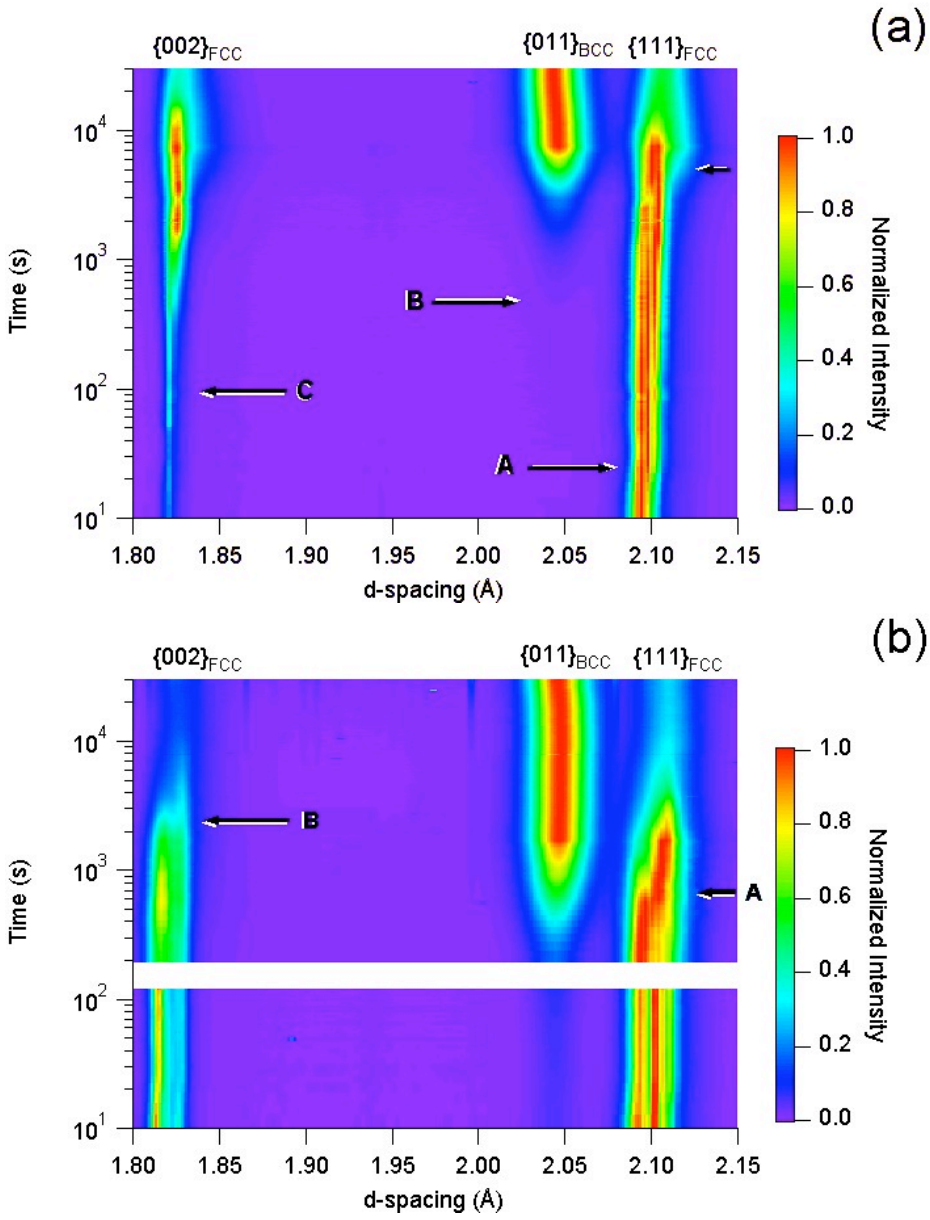

Figure 2. Image representations of diffraction data from two samples subjected to similar heat treatment are shown. In this image, the blue color corresponds to the background intensity and the maximum intensity is given by the red color. (a) Sample 1: Arrow A on $\{111\}_{FCC}$ line corresponds to onset of peak splitting; arrow B on $\{011\}_{BCC}$ correspond to the initiation of austenite to ferrite transformation; arrow C on the $\{002\}_{FCC}$ corresponds to the increase in the width of diffraction peak. (b) Sample 2: The blank white region in the image corresponds to absence of measurement due to a change in integration time. The arrow A on $\{111\}_{FCC}$ diffraction line indicates a rapid rate of change of the diffraction peaks and arrow B on $\{002\}_{FCC}$ indicates a similar change.

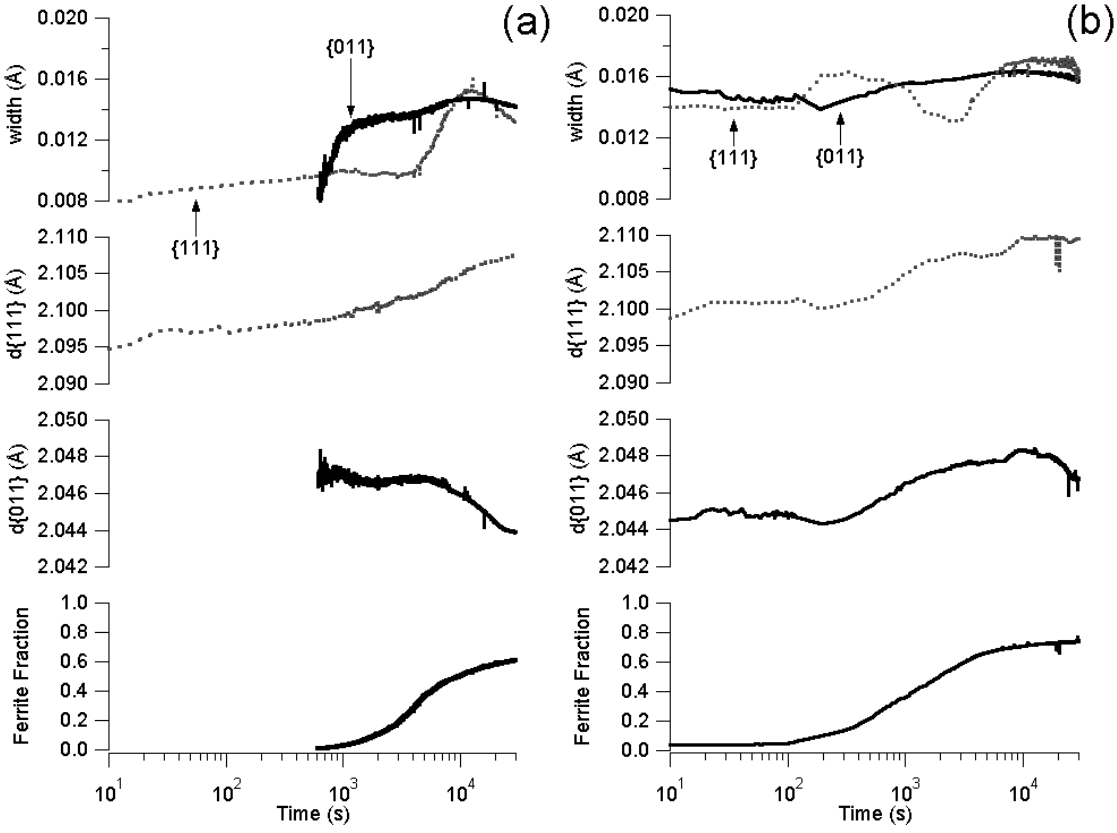

Figure 3. Results of data analysis from the diffraction data from (a) sample 1 and (b) sample 2 are summarized. The interplanar spacing of {111}FCC and {011}BCC, corresponding Gaussian width of the diffraction peaks, and the ferrite fraction calculated based on area fraction of the $\{111\}_{FCC}$ and $\{011\}_{BCC}$ diffraction peaks.

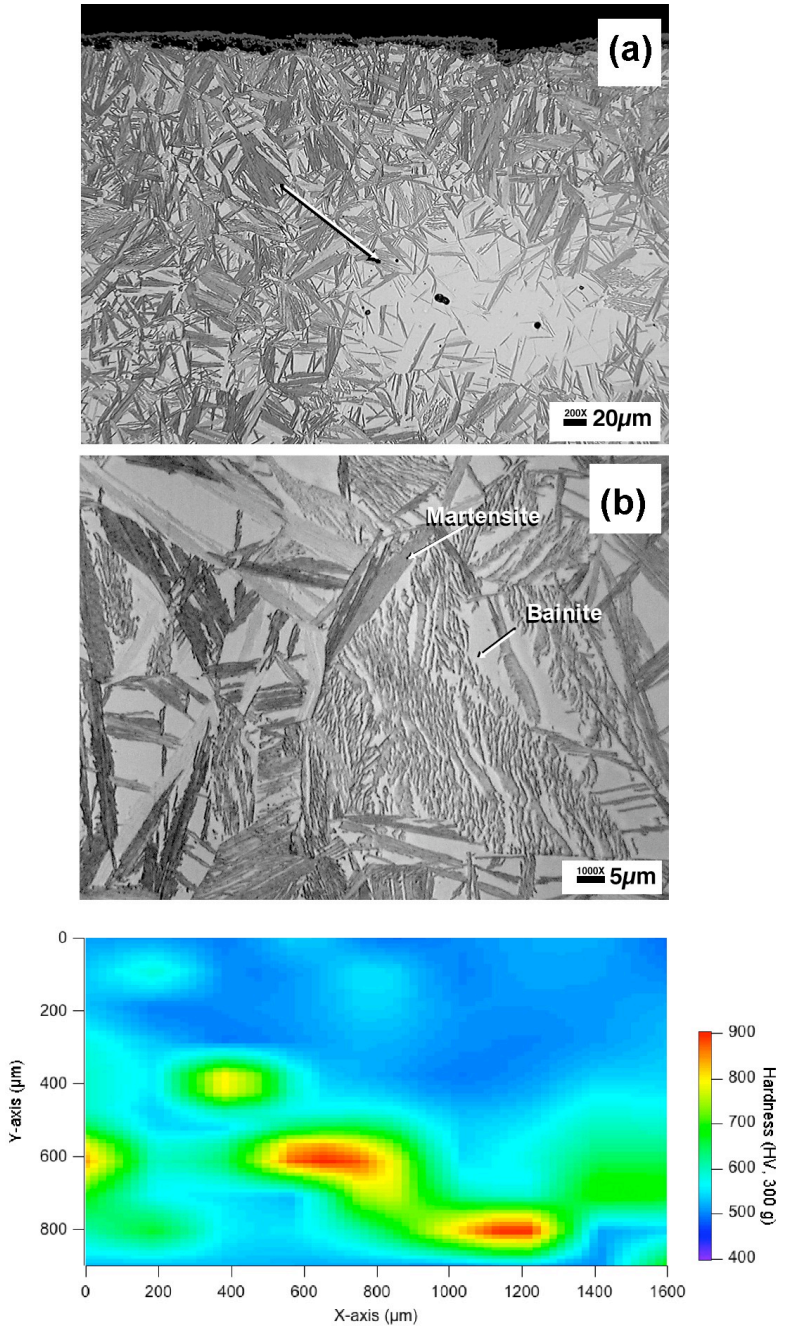

Figure 4. **Optical micrographs showing the overall microstructure at different magnifications are presented. (*a*) Low magnification micrograph shows a large island of untransformed region (marked by arrow). The micrograph also shows small amount of oxide on the surface of the sample (*b*) Higher magnification micrograph shows the presence of martensitic and bainitic microstructure with small blocks of untransformed region. (*c*) Spatial Vickers hardness variation in the sample shows the presence of hard and soft regions.**

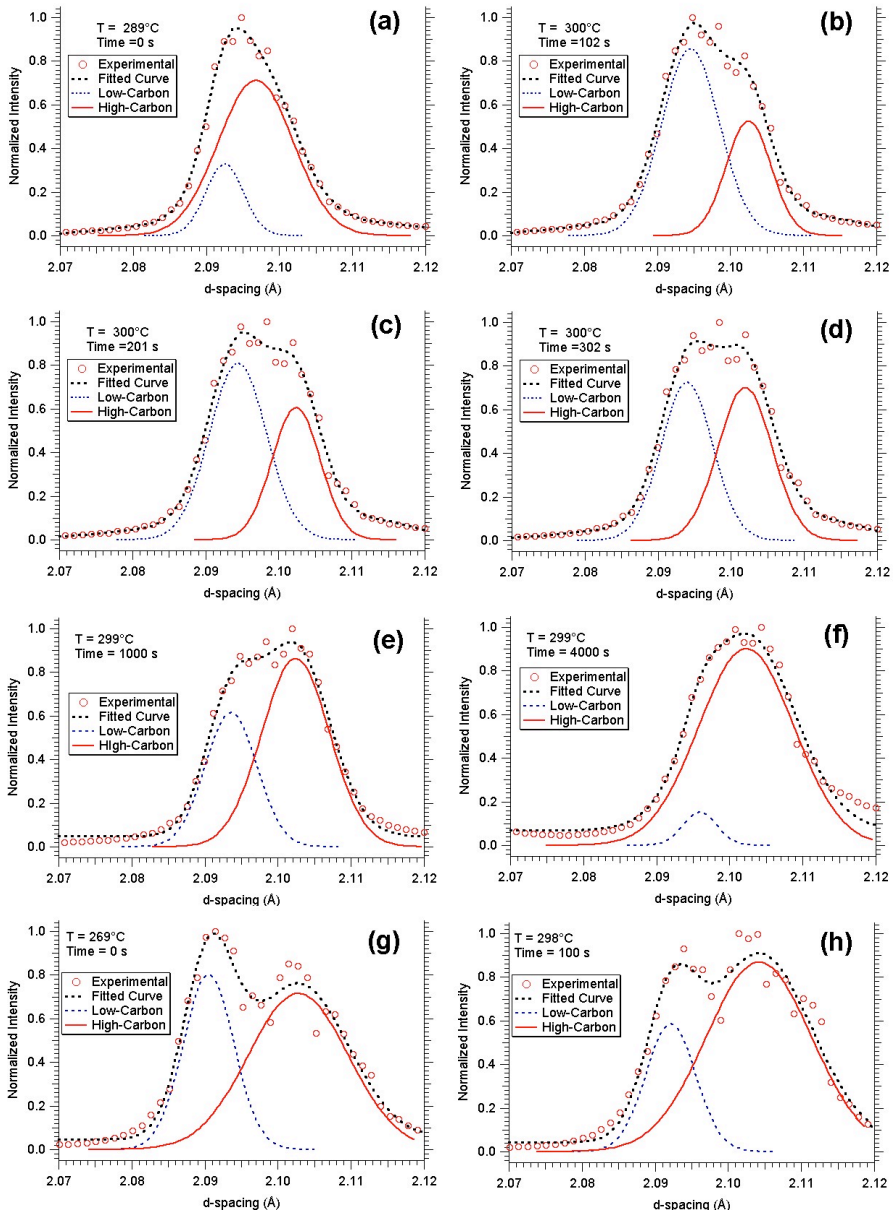

Figure 5. Analyses of $\{111\}_{FCC}$ diffraction peaks measured at different time intervals from sample 1 during isothermal holding at 573 K are shown with the fitted peaks with a Gaussian peak shape. (a) The diffraction peaks from 0 second shows the onset of peak splitting. Diffraction peaks at (b) 102, (c) 201 and (d) 302 seconds into isothermal hold at 573 K showing the onset and development of peak splitting. The diffraction data obtained after the ferrite transformation at (e) 1000 and (f) 4000 seconds show the reduction of low-carbon austenite fraction. The data from sample 2 at (g) 0-s into isothermal hold shows the presence of peak splitting as well as (h) reduction of low-carbon austenite peak intensity after 100-s hold.

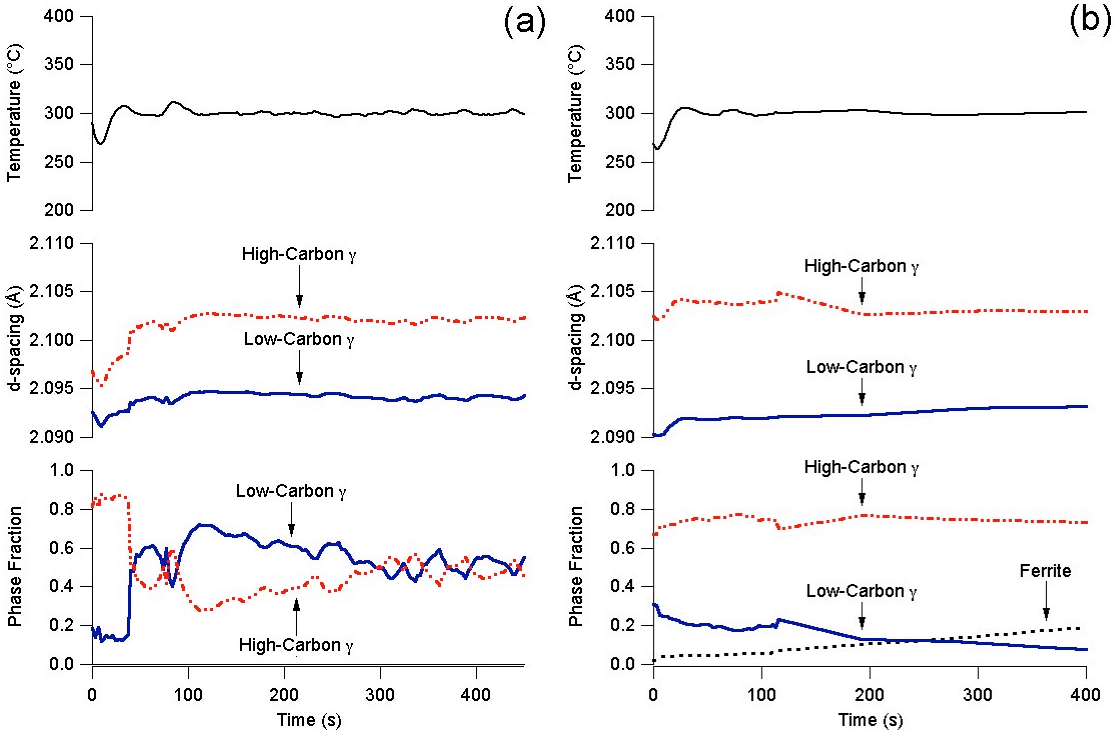

Figure 6. (a) Analysis of $\{111\}_{FCC}$ diffraction splitting at early stages of isothermal hold at 573 K before the onset of ferrite transformation from sample 1. Measured temperature, d-spacing of low- and high-carbon austenite and phase fractions of the of low- and high-carbon austenite as a function of time. (b) Similar analysis on data from sample 2 shows the reduction of low-carbon austenite fraction with increase in ferrite fraction.

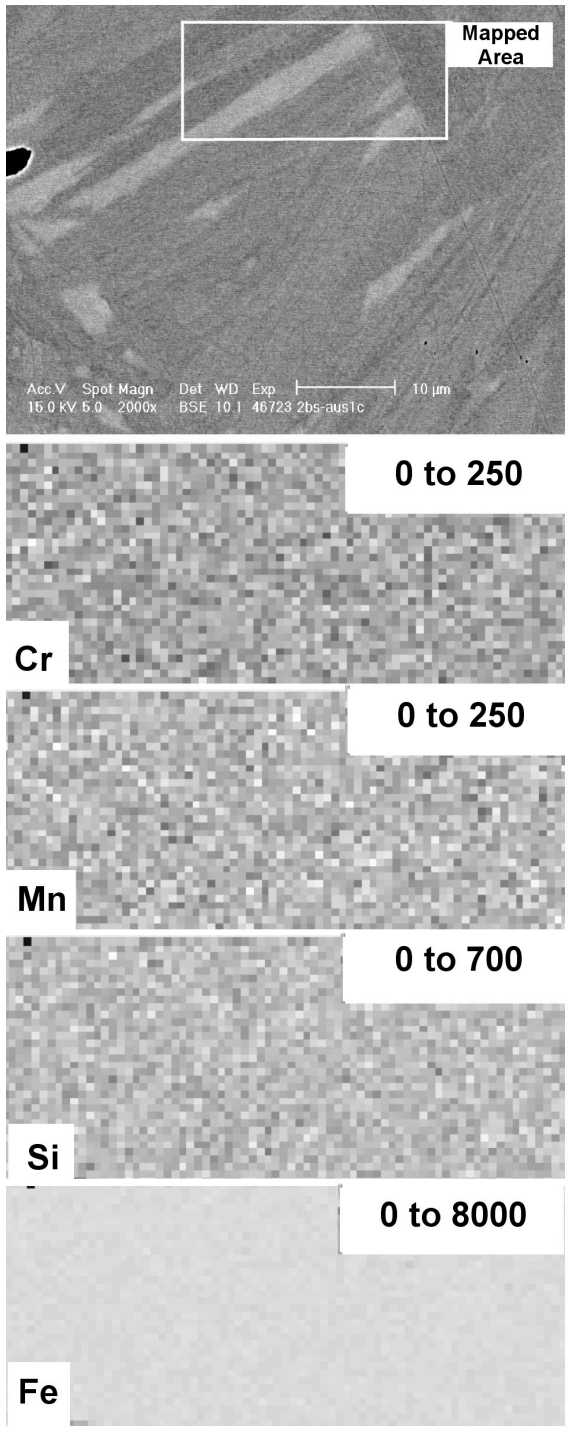

Figure 7. Results of energy dispersive X-ray spectrum analysis from the sample after the heat treatment at 573 K shows no large compositional gradients with reference to substitutional alloying additions Cr, Si and Mn. The gray scale image contrast ranges to minimum of zero and maximum of intensity ranges quoted in the maps.

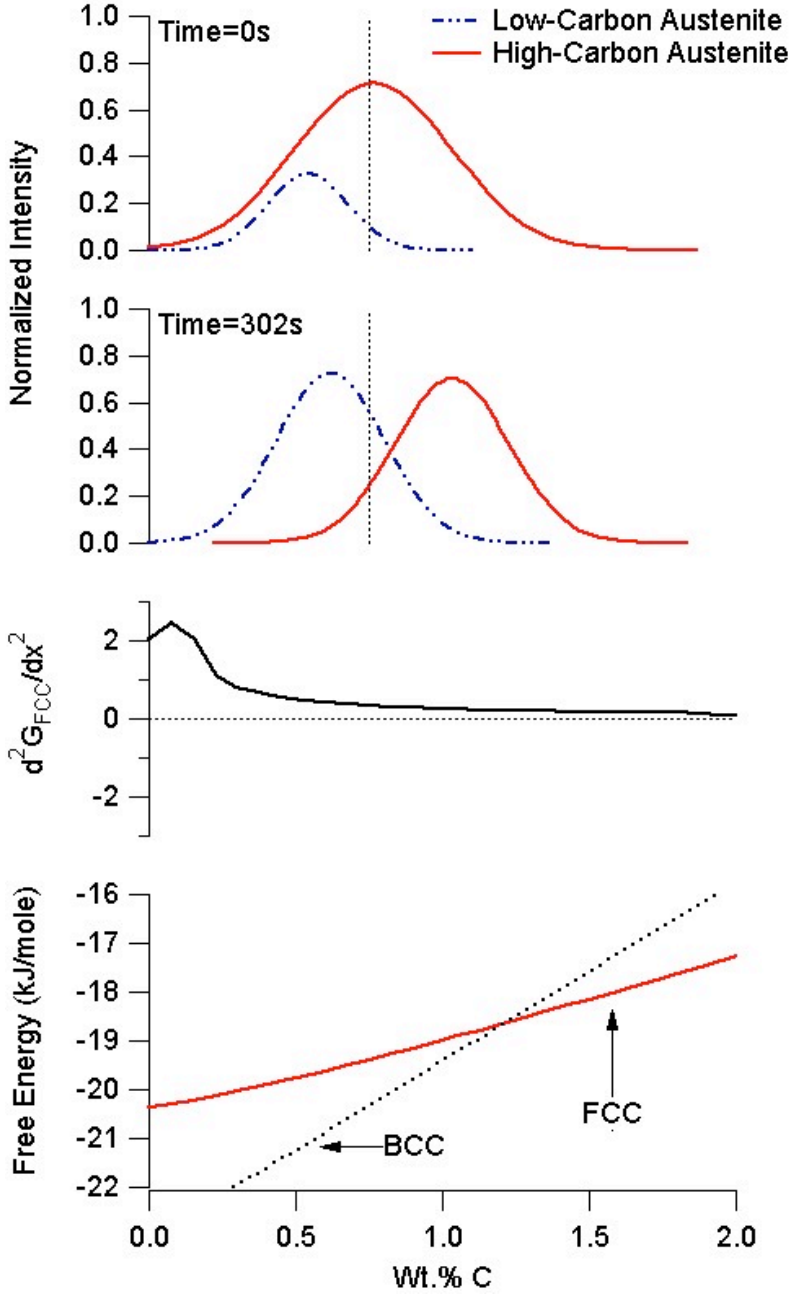

Figure 8. Comparison of the measured diffracted intensities from low- and high-carbon austenite at time 0- and 302-seconds with reference to calculated molar Gibbs free energy of the austenite and ferrite as a function of carbon concentration. The nominal carbon concentration of the alloy is also shown. The plots also show the second derivative of the Gibbs free energy of austenite as a function of carbon concentration in the austenite.

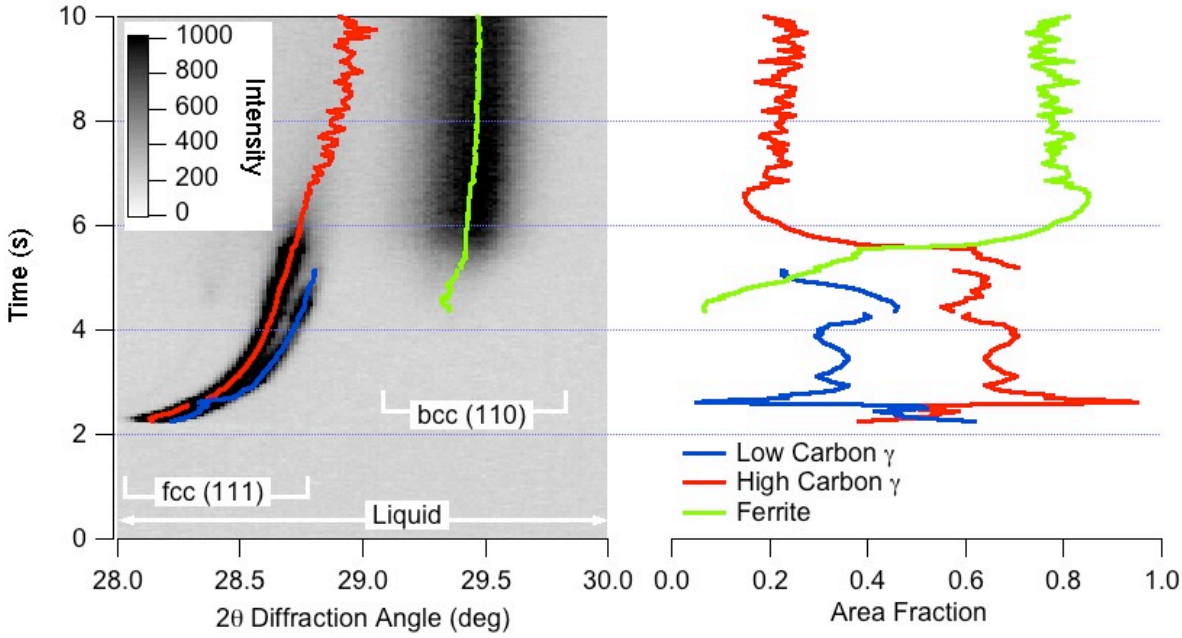

Figure 9. In-situ X-ray diffraction measurements taken at 0.05-second intervals during rapid cooling of a Fe-C-Al-Mn steel weld and the analyses of the data: The left side of the figure is the image representation of measured diffraction intensity (white background, black high intensity) during rapid cooling from the liquid state. The image is overlaid with the peak position of two austenite peaks as well as the ferrite peak position. The right side of the figure shows the calculated area fraction from peak area as a function of weld cooling time. During the initial stages (from 2.0 to 2.6 seconds) of measurements, the weld cools rapidly and may have averaging effect. The rate of change of temperature can be visualized by the change in slope of the 2θ with time.